Model-Based Quantitative Analysis of a Capacitive Cell Balancing Technique using SoC Estimator

Syed Bilal Javed[1], Ali Arshad Uppal[1], Muhammad Rizwan Azam[1], Khurram Shehzad[1] and Qadeer Ahmed[2]

***Abstract*— In a battery management system (BMS), cell balancing is an essential function to improve the performance and safe operation of batteries. In the literature, the performance of various cell balancing techniques has been analyzed by assuming ideal circuit parameters. In this paper, model-based quantitative analysis of a capacitive active cell balancing technique with static and dynamic parameters has been presented. A mean current modeling approach is employed to describe energy transfers between battery cells for long charge/discharge operations. The expression of mean current of cell balancing architecture is derived by considering the actual circuit parameters and validated with the simulation results. Moreover, the Kalman filter is designed to estimate the state of charge (SoC), as the efficacy of any balancing architecture mainly relies on the accurate estimation of SoC. The impact of circuit parameters on the performance of the active cell balancing technique has been investigated by performing a detailed sensitivity analysis. The results of sensitivity analysis show that the actual circuit parameters have a significant impact on the efficiency and balancing time of each technique. The efficacy of SoC estimator in cell balancing architecture is also discussed in detail.**

I. INTRODUCTION

Lithium-ion cells are affected by imbalances in capacity and state of charge (SoC) when connected in series. The imbalance is mainly caused either due to the internal sources (i.e., manufacturing variations, differences in internal impedances and variations in self discharge rate) or external sources (i.e., thermal effects) [1]. Various cell balancing architectures including passive and active circuits are employed in literature to overcome this issue [2]. Active balancing circuits are more efficient and provide fast energy transfer between cells. Herein, the energy is actively transferred between cells to get an equilibrium energy level during both charging and discharging processes. The active balancing circuits available in the literature differ in terms of energy storage elements (i.e., inductors, capacitors and transformers) and their interconnecting architecture [3], [4].

In most of the literature, c.f., [1], [4]–[8], performance of these techniques is compared by assigning an appropriate mark to different parameters like balancing time, circuit complexity, and efficiency, that gives a qualitative indication of the balancing architecture performance. Since these requirements depend on the field of application, selecting an optimal balancing architecture and the most suitable electronic component parameters pose a great challenge. Therefore, the analysis conducted in the above literature is not sufficient to highlight the effectiveness of different proposed solutions. In this regard, some of the recent literature also covers a quantitative analysis of active cell balancing techniques. In [3], the mean average current modeling approach is used to evaluate the performance of active cell balancing circuits. The average current models are simplified by ignoring the static and dynamic parameters of the active cell balancing architectures. A generalised analytical model is used in [9] to calculate the performance of various balancing architectures on the basis of balancing time and energy losses as a function of efficiency and the initial charge imbalance. However, an in-depth analysis is required to determine the effect of balancing circuit parameters and their connecting architecture on these performance measures.

In any cell balancing technique, an accurate estimation of SoC has a paramount importance. The available literature considers coulomb counting (CC) method for SoC estimation. The CC technique simply integrates the charging/discharging current to estimate the SoC and is susceptible to various source of errors. The error is accumulated in the estimation due to noise in the current measurement, uncertainty in battery capacity and model parameters, and the need for accurate knowledge of the initial SoC value [10], [11]. On the contrary, the Kalman filter based methods provide an accurate estimation of SoC value in the presence of measurement noise and uncertainties [12]. To the best of authors' knowledge, no literature considers Kalman filter based SoC estimation in the qualitative or quantitative analysis of active balancing circuits.

The aim of this paper is to provide a model-based quantitative analysis for the performance evaluation of a capacitive active cell balancing circuit. In the literature, the analysis is usually performed by assuming ideal circuit parameters. However, in this paper, actual static and dynamic parameters like resistances of cells, switch and energy storage elements, diode forward voltage drop and dead time have been considered for analysis. A mean current modeling approach is employed to describe energy transfers between battery cells for long charge/discharge operations. Moreover, a Kalman filter is designed to accurately estimate the SoC of each cell. Furthermore, sensitivity analysis is performed to assess the

*This work was not supported by any organization

S. B. Javed[1], A. A. Uppal[1], M. R. Azam[1] and K. Shehzad[1] are with the Department of Electrical and Computer Engineering, COMSATS University Islamabad, Islamabad 44000, Pakistan. syedbilal@comsats.edu.pk, ali_arshad@comsats.edu.pk, rizwan.azam@comsats.edu.pk, khurram.shehzad@comsats.edu.pk

[2]Qadeer Ahmed is with the Department of Center for Automotive Research, The Ohio State University, Columbus, OH 43210 USA ahmed.358@osu.edu

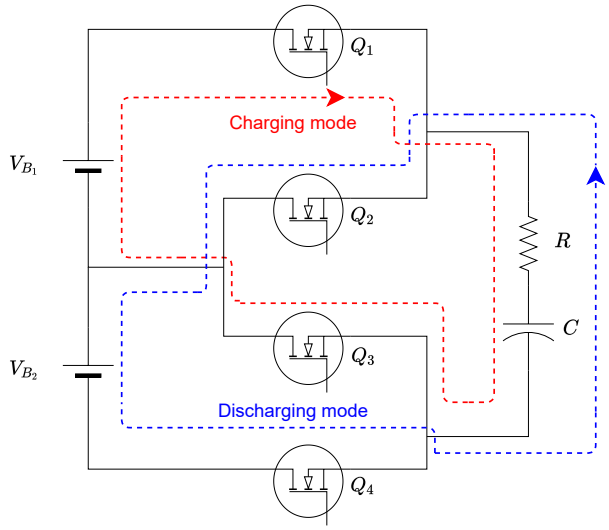

Fig. 1: Switching capacitor cell-balancing technique

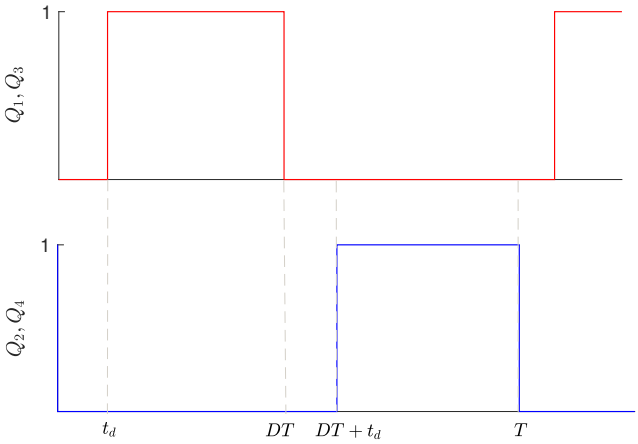

Fig. 2: Control algorithm for switches

impact of circuit parameters on the performance of the active cell balancing technique.

The rest of the paper is organised as follows: The capacitive cell balancing circuit model and equivalent circuit model (ECM) of the cell are presented in Section II. Section III describes the design of a Kalman filter for SoC estimation. A discussion then follows on the impact of real circuit elements on the performance of a capacitive balancing architecture in Section IV. Finally, the paper is concluded in Section V.

II. Model Description

There are numerous capacitor based cell balancing techniques such as switched capacitor (SC), double-tiered capacitor and flying capacitor configurations. These techniques employ capacitor as an energy storage element to transfer the charge between the cells. In the SC architecture, $2n$ switches and $n-1$ capacitors are required to balance a battery pack having n series-connected cells. In this paper, a simple architecture comprising one capacitor and two series-connected cells is considered to formulate the model equations, as shown in Fig. 1. These model equations can be generalized for a n series-connected cells battery pack, as the transfer of charge among two adjacent cells always require one capacitor. Moreover, this analysis can be extended to the other capacitor based cell balancing architectures.

The analysis is performed by considering the internal resistance (R_o) of the second-order equivalent circuit model of Lithium-ion batteries (LIB), capacitor parasitic resistance (R_c), drain-source on-state resistance (R_{ds}) and dynamic parameters of the switches. The switches ($Q_1 = Q_3 = Q$, $Q_2 = Q_4 = \bar{Q}$) are controlled by a simple pulse-width modulation (PWM) signal having duty cycle (D) and switching period (T), as shown in Fig. 2. While V_{B_1} and V_{B_2} represent the cells having highest and lowest voltages, respectively. The SC architecture has three operating modes i.e., charging and discharging modes of the capacitor, and operation during the dead time (t_d). During the charging mode, the current flows from the highest voltage cell V_{B_1} to the capacitor and it begins to charge. Afterward, t_d is considered between the opening of $Q_1 - Q_3$ and the closing of $Q_2 - Q_4$ or vice versa to prevent undesired short circuits amongst the cells. The discharge mode begins when the switches Q_2 and Q_4 are turned on and the capacitor starts to discharge and transfers the stored charge to the lowest voltage cell V_{B_2}. Under steady state condition, the voltage across the capacitor during each mode is given as

$$v_c(t) = \begin{cases} V_1, & 0 \le t \le t_d, \\ V_{B_1} + (V_1 - V_{B_1})e^{-(t-t_d)/\tau}, & t_d \le t \le DT, \\ V_2, & DT \le t \le DT + t_d, \\ V_{B_2} - (V_{B_2} - V_2)e^{-(t-DT-t_d)/\tau}, & (DT + t_d) \le t \le T, \end{cases} \tag{1}$$

where $\tau = RC$ represents the voltage transient time constant and R is the net resistance of the circuit. During charging and discharging modes, two switches are included, therefore, R is characterized as

$$R = R_c + 2R_{ds} + R_o \tag{2}$$

A. Mean balancing Current

Generally, the transfer of charge between cells occurs at high rates per second (f) with repeated cycles, and the net transfer of charge by balancing currents in one switching cycle is negligibly smaller as compared to the charge stored in battery cells. Thus, the mean averages of current in a switching period (T) can be used to represent the current trajectories. The mean value of capacitor current can be expressed as

$$\tilde{I} = \frac{\Delta Q}{T} = \frac{C}{T}\Delta V, \tag{3}$$

where ΔV is the voltage ripple and C is the capacitor size. It is evident in (3) that $\tilde{I}$ is highest at the maximum ripple

voltage condition for the SC network. The analysis of (1) shows that the maximum ripple voltage occurs at $D = 0.5$ and it can be expressed as

$$\Delta V = (V_{B_1} - V_{B_2})\, Tanh\left(\frac{0.5T - t_d}{2\tau}\right) \tag{4}$$

Hence, the mean current for a single time interval of the length $T/2$ becomes

$$\tilde{I} = \frac{C}{T}(V_{B_1} - V_{B_2})\, Tanh\left(\frac{0.5T - t_d}{2\tau}\right) \tag{5}$$

This is the fundamental expression of $\tilde{I}$ which shows that the performance of SC network is a function of all parasitic, static and dynamic parameters. Moreover, it also includes switching frequency and cell imbalance voltages.

B. Efficiency and Balancing Time

The efficiency and cell balancing time are important performance metrics of a cell balancing architecture. These parameters are sensitive to the real conditions of the balancing network. The percentage efficiency of an active cell balancing technique is

$$\eta = \left[1 - \frac{\bar{P}_{losses}}{\bar{P}_{in}}\right] 100\%, \tag{6}$$

where $\bar{P}_{in}$ and $\bar{P}_{losses}$ are average input power and average power losses due to conduction and switching. The conduction losses during one switching period are

$$\bar{P}_{con} = 2\tilde{I}^2 R \tag{7}$$

The switching losses during turn-on and turn-off are computed by using the piece-wise linear functions shown in Fig. 3. The switching losses of switch Q_1 due to rise time and fall time are

$$\begin{aligned} P_{sw1_{tr}} = &\int_{0.2tr}^{0.3t_r} \left(\frac{0.1V_{B_1} - V_{B_1}}{0.1t_r}(t - 0.2t_r) + V_{B_1}\right) \quad \left(\frac{0.7I_2}{0.1t_r}(t - 0.2t_r)\right) dt \\ &+ \int_{0.3t_r}^{t_r} \left(\frac{0.009V_{B_1} - 0.1V_{B_1}}{0.7t_r}(t - 0.3t_r) + 0.1V_{B_1}\right) \left(\frac{I_2 - 0.7I_2}{0.7t_r}(t - 0.3t_r)\right) dt, \end{aligned} \tag{8}$$

$$\begin{aligned} P_{sw1_{tf}} = &\int_{0}^{0.1t_f} \left(\frac{0.9V_{B_1} - 0.009V_{B_1}}{0.1t_f}t + 0.009V_{B_1}\right) \quad \left(\frac{0.7I_1 - I_1}{0.1t_f}t + I_1\right) dt \\ &+ \int_{0.1t_f}^{t_f} \left(\frac{VB_1 - 0.9V_{B_1}}{0.9t_f}(t - 0.1t_f) + 0.9V_{B_1}\right) \left(\frac{-0.7I_1}{0.9t_f}(t - 0.1t_f) + 0.7I_1\right) dt, \end{aligned} \tag{9}$$

where I_1 and I_2 can be found by using (1), and it is given as

$$\begin{aligned} I_1 &= \frac{V_{B_1} - V_{B_2}}{R}\left[\frac{1}{1 + exp\left(\frac{DT - t_d}{\tau}\right)}\right], \\ I_2 &= \frac{V_{B_1} - V_{B_2}}{R}\left[\frac{exp\left(\frac{DT - t_d}{\tau}\right)}{1 + exp\left(\frac{DT - t_d}{\tau}\right)}\right]. \end{aligned} \tag{10}$$

Similarly, the switching losses for other switches due to rise time and fall time are computed.

C. Equivalent Circuit Model of the Battery Cell

The second order Randle model of [13] is selected to represent the equivalent circuit of the cell. The circuit diagram is shown in Fig. 4. The mathematical model is adapted from [13], [14] and is represented as

$$\begin{aligned} \dot{x} &= Ax + Bi + w(t), \\ v_t &= Cx + Di + v_{OC_0} + \varphi(t), \end{aligned} \tag{11}$$

where $x \in \Re^3$ represents the state vector, $A \in \Re^{3\times 3}$ is the system matrix, $B \in \Re^3$ is the input matrix, i is the charging

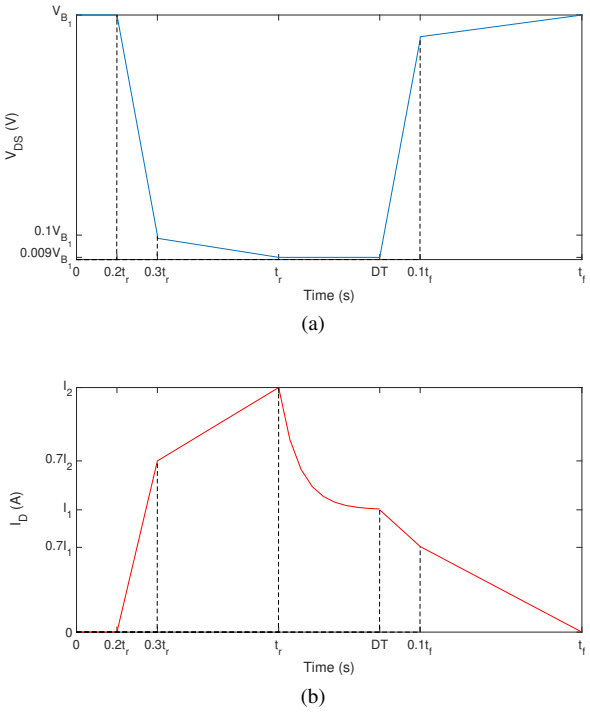

Fig. 3: Piece-wise function of Q_1 during switching period

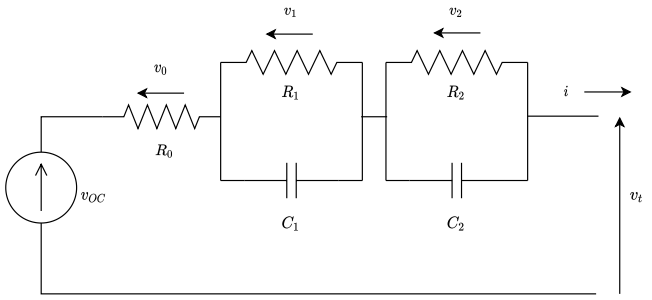

Fig. 4: Equivalent circuit of the cell.

or discharging input current, v_t is the terminal voltage representing the output of the cell, v_{OC_0} is the value of the open circuit voltage v_{OC} at zero state of charge (SoC), C is the output matrix, D is the direct transition matrix, and $w(t)$ and $\varphi(t)$ represent the process and measurement noises, respectively.

The components of the state space model in (11) are given as

$$
\begin{aligned}
x &= \begin{bmatrix} v_1 & v_2 & SoC \end{bmatrix}^T, \\
A &= \begin{bmatrix} -\dfrac{1}{R_1C_1} & 0 & 0 \\ 0 & -\dfrac{1}{R_2C_2} & 0 \\ 0 & 0 & 0 \end{bmatrix}, \\
B &= \begin{bmatrix} \dfrac{1}{C_1} & \dfrac{1}{C_2} & -\dfrac{1}{\zeta} \end{bmatrix}^T, \\
C &= \begin{bmatrix} -1 & -1 & m \end{bmatrix}, \\
D &= -R_0,
\end{aligned}
$$

where v_i, R_i, C_i, $i = \{1,2\}$ are the voltage, resistance and capacitance of the RC networks of the equivalent circuit shown in Fig. 4, respectively, ζ is the nominal capacity of the cell, m is the slope of v_{OC} and SoC curve, and R_0 is the internal resistance of the cell.

III. SOC Estimator

The cell model given in (11) is employed to design the discrete time Kalman Filter (DKF) for estimating SoC. The first step is to discretize (11) with sampling time dt to yield

$$
\begin{aligned}
x_k &= F_{k-1} + Gi_{k-1} + w_{k-1}, \\
y_k &= C_k + Di_k + \phi_k,
\end{aligned} \tag{12}
$$

where $F = I_3 + dtA$, $G = dtB$, $y_k = v_t - v_{OC_0}$ and w_k and ϕ_k are white, zero-mean, uncorrelated noise processes with known covariance matrices $\mathscr{Q}_k$ and $\mathscr{R}_k$, respectively, which are characterized as (cf. [15])

$$
\begin{aligned}
&w_k \sim (0, \mathscr{Q}_k), \quad v_k \sim (0, \mathscr{R}_k), \quad E\left[w_k w_j^T\right] = \mathscr{Q}_k \delta_{k-j} \\
&E\left[v_k v_j^T\right] = \mathscr{R}_k \delta_{k-j}, \quad E\left[v_k w_j^T\right] = 0,
\end{aligned}
$$

where the kronecker delta function $\delta_{k-j} = 1$ if $k = j$ and $\delta_{k-j} = 0$ if $k \neq j$.

The steps involved in the implementation of DKF are presented in algorithm 1.

Algorithm 1 Discrete time Kalman Filter Implementation

1: **Initialize:** The state vector ($\hat{x}$) and estimation error covariance matrix ($P \in \Re^{3\times 3}$) of the DKF are initialized at $k = 0$ as

$$
\begin{aligned}
\hat{x}_0^+ &= E(x_0), \\
P_0^+ &= E\left[\left(x_0 - \hat{x}_0^+\right)\left(x_0 - \hat{x}_0^+\right)^T\right],
\end{aligned} \tag{13}
$$

where $+$ denotes the posteriori estimate, which takes into account the current measurement, and E represents the expected value.

2: **Predict and Update:** For $k = 1, 2, \ldots$, the DKF predicts and subsequently corrects/updates the states based on the current measurement as follows

a. **Predict:** The gain of the DKF K, P and $\hat{x}$ are predicted by the following set of equations

$$
\begin{aligned}
P_k^- &= F_{k-1} P_{k-1}^+ F_{k-1}^T + \mathscr{Q}_{k-1}, \\
K_k^- &= P_k^- C_k^T \left(C P_k^- C^T + \mathscr{R}_k\right)^{-1}, \\
\hat{x}_k^- &= F_{k-1} \hat{x}_{k-1}^+ + Gi_{k-1},
\end{aligned} \tag{14}
$$

where $-$ denotes the a-prior estimate, which does not depend on the current measurement

b. **Update:** By using the current measurement $\hat{x}$ and P are updated as

$$
\begin{aligned}
\hat{x}_k^+ &= \hat{x}_k^- + K_k\left[y_k - \left(C_k \hat{x}_k^- + Di_k\right)\right], \\
P_k^+ &= (I_5 - K_k C) P_k^- (I_5 - K_k C)^T + K_k \mathscr{R}_k K_k^T.
\end{aligned} \tag{15}
$$

IV. Results and Discussion

In this section, simulation results are presented to show the impact of real conditions on the performance of the balancing architecture. The practical scenario is presented by incorporating the following practical considerations.

- 4.4-Ah Boston Power Sonata cells are considered and the main characteristic parameters of cells are given in Table I.
- The static parameters like resistances of energy storage elements, switches and battery cells are considered.
- The dynamic parameters in the form of dead time, rise time and fall time are also included.
- An affine approximation of the SoC vs OCV curve is used for the linear model of the cell, cf. 11. Where the parameter $m = 0.0051$ and $v_{OC_0} = 3.6971$.
- The imbalance in battery cells is presented by considering distinct SoC for each cell.
- The noises are considered during the simulation study to investigate their impact on the performance of the SoC estimator. These noises are classified into the process noise (w) and measurement noise (ϕ). The zero-mean Gaussian white noise with a variance of 10^{-2} is assumed for both process and measurement noises.

The implementation of the proposed scheme is shown in Fig. 5. To investigate the impact of static and dynamic parameters on the performance of the SC architecture, a real time

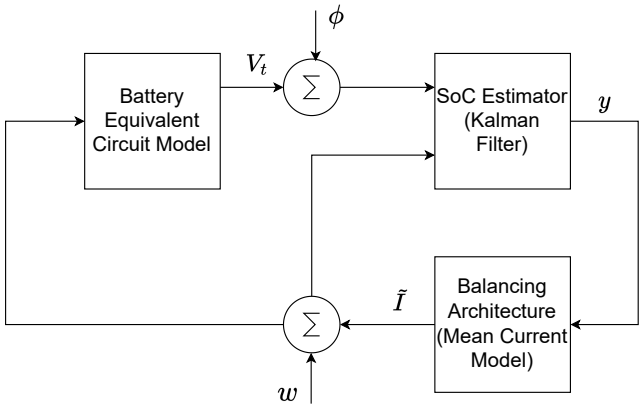

Fig. 5: Proposed implementation scheme

TABLE I: List of Parameters

Parameters of Boston Power Sonata 4400 cell (cf. [14]).			
ζ	4.4 Ah	R_1	18.6 mΩ
R_2	4 mΩ	C_1	69.176×10^3 F
C_2	138 F	R_o	44.1 mΩ
Parameters used in the balancing architecture.			
Q_i	5.3 mΩ	C	47 μ F
R_c	10 mΩ	f	50 kHz
t_d	2 μs	R_{ds}	5.3mΩ
t_r	72 ns	t_f	8 ns

scenario is incorporated by considering that two cells are imbalanced by $300mV$ and their voltages are $4.0V$ and $3.7V$, respectively. The parameters of cell balancing architecture are shown in Table I. The impact of real parameters on the performance of the cell balancing architecture is determined by computing the deviation of η and $\tilde{I}$ from the ideal values. The percentage changes $\Delta\eta\%$ and $\Delta\tilde{I}\%$ are computed as

$$\Delta\eta\% = \frac{\eta(Real) - \eta(Ideal)}{\eta(Ideal)}, \tag{16}$$

$$\Delta\tilde{I}\% = \frac{\tilde{I}(Real) - \tilde{I}(Ideal)}{\tilde{I}(Ideal)}, \tag{17}$$

where $\eta(Real)$ and $\eta(Ideal)$ are the efficiency of real and ideal networks, respectively. While $\tilde{I}(Real)$ and $\tilde{I}(Ideal)$ are the average currents of real and ideal circuits, respectively. In Fig. 6a, it is evident that the average current reduces with the increase in parasitic and on-state resistances of switches. Moreover, the dead time also affects the average current and a significant deviation can be observed from the ideal scenario at large values of resistances. The dead time reduces the effective duty cycle which leads to the reduction of balancing current, so it slows down the cell balancing speed. Similarly, the deviation of efficiency from the ideal balancing network is observed in Fig. 6b. The effect of dynamic parameters like rise time (t_{rise}) and fall time (t_{fall}) on the efficiency of the SC network is also investigated. The switching losses increase with the increase in rise and

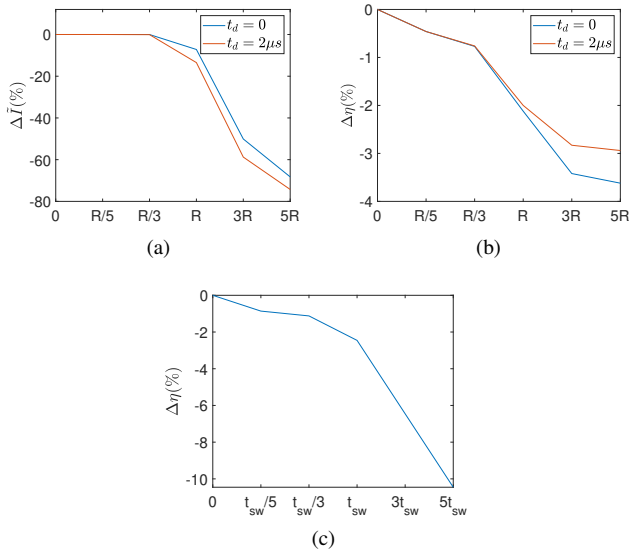

Fig. 6: Effect of static and dynamic parameters on the performance of SC balancing architecture

fall times, resulting in a low efficiency at higher values of switching time, as shown in Fig. 6c.

The speed of cell balancing is another important performance metric of a cell balancing architecture. A DKF is designed for the estimation of the SoC of each battery cell to determine the performance of a cell balancing architecture. The process and measurement noises are considered in the balancing currents and the terminal voltages of battery cells, respectively.

To show the effectiveness of the estimation, the battery cells and the DKFs are initialized with different initial conditions. The discharging cell (cell 1) and its estimator are initialized as

$$x(0) = \begin{bmatrix} 0 & 0 & 80 \end{bmatrix}^T, \hat{x}_0 = \begin{bmatrix} 0 & 0 & 85 \end{bmatrix}^T,$$

where as the other cell (cell 2), which is being charged and its estimator are assigned following initial condition vectors

$$x(0) = \begin{bmatrix} 0 & 0 & 60 \end{bmatrix}^T, \hat{x}_0 = \begin{bmatrix} 0 & 0 & 55 \end{bmatrix}^T.$$

It can be seen from Fig. 7 that the DKFs quickly converge to the true values of SoC. The superiority of DKF as compared to the CC method is also presented in Fig. 7. It can be observed that the CC method fails to give the correct estimate in case of unknown initial condition. On the contrary, the DKF yields an accurate estimation of the SoC in the presence of process and measurement noises. For the tuning of the DKF, $\mathscr{Q} = diag\{0,0,0\}$ and $\mathscr{R} = 10^{-1}$.

The designed DKFs are integrated with the cell balancing architecture to investigate the impact of real conditions on the performance of the balancing architecture. The impact of static and dynamic parameters is also evident in the cell balancing speed, as shown in Fig. 8. The simulation results show that the convergence time of SoC and OCV is higher

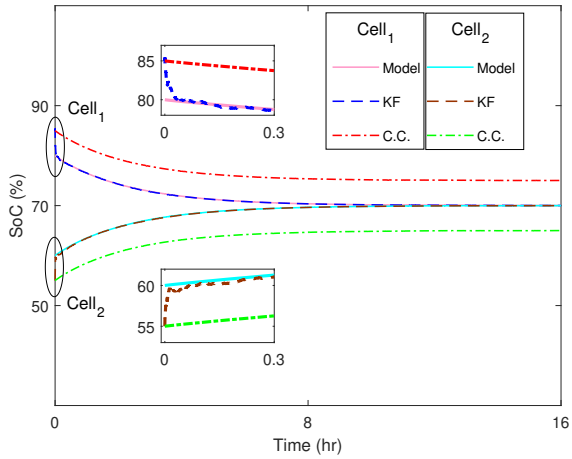

Fig. 7: Comparison of SoC estimators

in non-ideal conditions. Thus, the cell balancing speed is low in a practical balancing architecture as compared to the ideal network. These results show that the real conditions of the cell balancing network have a significant impact on the cell balancing efficiency and time.

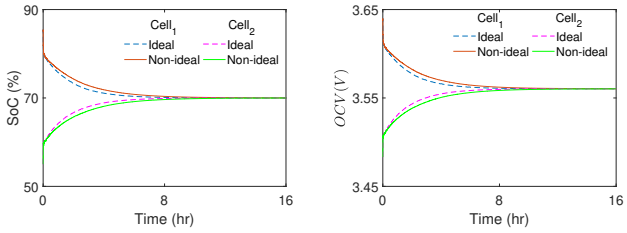

(a) (b)

Fig. 8: Effect of static and dynamic parameters on cell balancing speed

V. Conclusion

In this manuscript, a capacitive cell balancing architecture is analyzed by considering real conditions. A mean current model has been formulated to perform the sensitivity analysis. It is observed that the efficiency and cell balancing speed are sensitive to the real parameters like resistances of switches, cell and parasitic components. The dynamic parameters such as rise time, fall time and dead time also affect the performance of the cell balancing architecture. Moreover, it has been shown that an accurate SoC estimator is essential to determine the cell balancing time. It has been shown that the Kalman filter results are better as compared to Coulomb counting method.

One of the possible extensions of the current work is the development of the nonlinear equivalent circuit model based SoC estimation algorithm, which can account for the dependence of cell parameters on SoC and operating temperature. Moreover, SC based balancing architecture can be compared with inductor and transformer based balancing architectures.

References

[1] J. Cao, N. Schofield, and A. Emadi, "Battery balancing methods: A comprehensive review," in *2008 IEEE Vehicle Power and Propulsion Conference*. IEEE, 2008, pp. 1–6.

[2] S. W. Moore and P. J. Schneider, "A review of cell equalization methods for lithium ion and lithium polymer battery systems," 2001.

[3]

[4] J. Carter, Z. Fan, and J. Cao, "Cell equalisation circuits: A review," *Journal of Power Sources*, vol. 448, p. 227489, 2020.

[5] Y. Hua, S. Zhou, H. Cui, X. Liu, C. Zhang, X. Xu, H. Ling, and S. Yang, "A comprehensive review on inconsistency and equalization technology of lithium-ion battery for electric vehicles," *International Journal of Energy Research*, vol. 44, no. 14, pp. 11 059–11 087, 2020.

[6] Y. Shang, B. Xia, C. Zhang, N. Cui, J. Yang, and C. C. Mi, "An automatic equalizer based on forward–flyback converter for series-connected battery strings," *IEEE Transactions on Industrial Electronics*, vol. 64, no. 7, pp. 5380–5391, 2017.

[7] J. Gallardo-Lozano, E. Romero-Cadaval, M. I. Milanes-Montero, and M. A. Guerrero-Martinez, "Battery equalization active methods," *Journal of Power Sources*, vol. 246, pp. 934–949, 2014.

[8] M. Daowd, N. Omar, P. Van Den Bossche, and J. Van Mierlo, "Passive and active battery balancing comparison based on matlab simulation," in *2011 IEEE Vehicle Power and Propulsion Conference*. IEEE, 2011, pp. 1–7.

[9] F. Baronti, R. Roncella, and R. Saletti, "Performance comparison of active balancing techniques for lithium-ion batteries," *Journal of Power Sources*, vol. 267, pp. 603–609, 2014.

[10] H. He, R. Xiong, X. Zhang, F. Sun, and J. Fan, "State-of-charge estimation of the lithium-ion battery using an adaptive extended kalman filter based on an improved thevenin model," *IEEE Transactions on vehicular technology*, vol. 60, no. 4, pp. 1461–1469, 2011.

[11] K. Movassagh, A. Raihan, B. Balasingam, and K. Pattipati, "A critical look at coulomb counting approach for state of charge estimation in batteries," *Energies*, vol. 14, no. 14, p. 4074, 2021.

[12] P. Shrivastava, T. K. Soon, M. Y. I. B. Idris, and S. Mekhilef, "Overview of model-based online state-of-charge estimation using kalman filter family for lithium-ion batteries," *Renewable and Sustainable Energy Reviews*, vol. 113, p. 109233, 2019.

[13] G. R. Fabio Codecà, Sergio M. Savaresi, "On battery state of charge estimation: a new mixed algorithm," in *17th IEEE International Conference on Control Applications, Part of 2008 IEEE Multi-conference on Systems and Control*, 2008, pp. 102–107.

[14] P. Spagnol, S. Rossi, and S. M. Savaresi, "Kalman filter soc estimation for li-ion batteries," in *2011 IEEE International Conference on Control Applications (CCA)*, 2011, pp. 587–592.

[15] D. Simon, "The discrete-time Kalman filter," in *Optimal State Estimation*. John Wiley & Sons, Ltd, 2006, pp. 121–148. [Online]. Available: https://onlinelibrary.wiley.com/doi/abs/10.1002/0470045345.ch5